On-chip dual-band waveguide Bragg filter with identical subnanometer-bandwidth stopbands near 1310 and 1950 nm wavelengths

Zhengrui Tu, Jianhao Zhang, Carlos Alonso-Ramos, Xavier Le Roux, Laurent Vivien, Eric Cassan

On-chip dual-band waveguide Bragg filter with identical sub-nanometer-bandwidth stopbands near 1310nm and 1950nm wavelengths

Zhengrui Tu*, Jianhao Zhang, Carlos Alonso-Ramos, Xavier Le Roux, Laurent Vivien, and Eric Cassan

Université Paris-Saclay, CNRS, Centre de Nanosciences et de Nanotechnologies, 91120, Palaiseau, France

* Corresponding author:
E-mail address: zhengrui.tu@universite-paris-saclay

Abstract

We propose the realization of an on-chip dual identical narrowband Bragg filter at ~1310nm and ~1950nm wavelengths simultaneously based on the silicon-on-insulator (SOI) platform. By taking advantage of a subwavelength corrugation behavior at large wavelengths and a huge difference in the mode areas of the involved modes at the two widely separated wavelengths, undesired diffraction losses are circumvented while achieving Bragg resonances at the two wavelengths simultaneously. A double corrugation Bragg grating rib waveguide filter is proposed, with two sets of gratings, the inner one close to the rib operating near 1310nm wavelength while the outer grating being designed to achieve a transmission dip around 1950nm. Introducing a proper lateral misalignment to the set of inner grating indents, a dual identical narrowband Bragg filter owning ~0.47nm 3dB bandwidth at ~1310nm and ~1950nm is achieved. The proposed design strategy based on SOI platform relies on a single-etching fabrication process and presents potential applications in all situations where equal-bandwidth filtering is needed in on-chip communications and sensing.

1. Introduction

Bragg gratings waveguide structures on different platforms, such as silicon-on-insulator (SOI), silicon nitride, III-V, etc., play a great role in various application fields, including lasers [1], modulators [2,3], filters [4,5], signal processing circuits [6], optical delay lines [7,8], on-chip sensors [9,10], wavelength division multiplexers [11]. Several types of Bragg waveguide gratings, such as phased-shift [9,10], apodized [7], Moiré [12], sampled [13], or cladding-modulated gratings [14-16], have been demonstrated and each of them can provide its own special advantages. The studies based on Bragg gratings are thriving in the past decades. Multiband operation is a valid option to significantly extend optical communication capacity [17]. However, there are few works only addressing how to successfully circumvent diffraction limitation resulting in achieving an on-chip dual identical narrowband Bragg filtering simultaneously at two separated far away wavelengths. A straightforward approach is to implement both gratings on the same waveguide simultaneously, but this is not without difficulty. Due to the huge difference between these involved wavelengths, the Bragg grating period for the longer wavelength can then be responsible for diffraction at the short aiming wavelengths, thus hindering the target dual function.

In this work, based on SOI platform, we fix as a typical example objective case where filtering at ~1310nm and ~1950nm with identical narrow stopbands are simultaneously needed. A rib waveguide geometry containing two sets of gratings is chosen (see Fig. 1 (a)) as in this type of waveguide, where a mode field can spread widely laterally in the slab, the introduction of corrugation that disturbs the profile of the guided mode is simpler than in a fully etched strip waveguide. One of the set of gratings (inner gratings), which is considered just close to the rib, is designed for ~1310nm Bragg wavelength operation. Another one is located far away enough to the rib (outer gratings) to generate the ~1950nm wavelength stopband. Section 2 describes the proposed methodology applied to obtain two stopbands with identical 3dB bandwidth (~0.47nm) at ~1310nm and ~1950nm over a ~1.3mm long rib slightly single-etched SOI waveguide. In section 3, simulation results are reported, demonstrating the soundness and the efficiency of proposed design strategy. Then, discussion and conclusion are given in section 4.

2. Principles and design

The proposed methodology is illustrated relying on a 220nm thick (H_{core}) SOI wafer case. Preliminarily, in order to obtain a waveguide that can well support a TE-like polarization mode within a broadband wavelength range

(covering the ~1310nm-~1950nm range in our case), a rib waveguide with rib width (W_{rib}) of 500nm and rib height (H_{rib}) of 100nm are chosen. The 3D schematic and 2D cross-section pictures of the rib waveguide are shown in Fig. 1(a) and Fig1. (b), respectively.

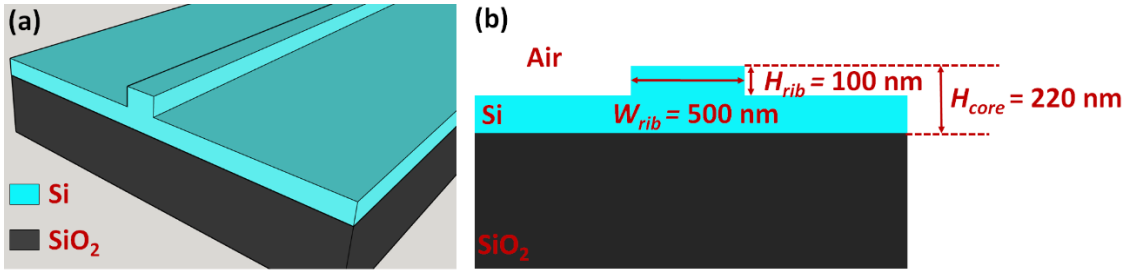

Fig. 1 (a) 3D schematic (b) 2D cross-section view of the SOI rib waveguide.

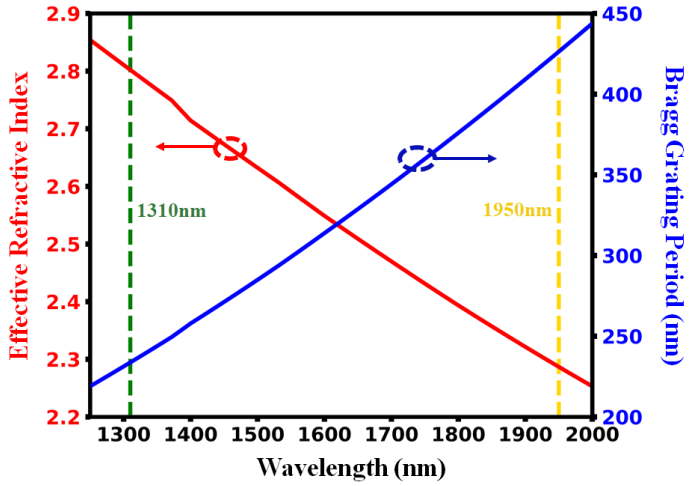

Fig. 2 Red curve: relationship between wavelength and effective refractive index; blue curve: relationship between wavelength and Bragg grating period.

Based on this rib waveguide structure, the effective refractive index for wavelengths ranging from 1250nm to 2000nm in TE-like foundational mode was calculated and the result is shown as the red curve in Fig. 2. According to the Bragg's law [18], the corresponding grating period for the 1st order Bragg wavelength can be derived from equation (1):

$$\Lambda = \frac{\lambda_B}{2n_{eff}} \tag{1}$$

where Λ is the grating period, λ_B is the 1st order Bragg wavelength, and n_{eff} is the effective refractive index at λ_B. In Fig. 2, the blue curve gives out the relationship between the Bragg grating period and light wavelength. Two dashed vertical lines are labeled: the green one corresponds to a stopband center wavelength of 1310nm (λ_{B-}) and the yellow one corresponds to a similar stopband wavelength of 1950nm (λ_{B+}). From Fig. 2, one can find that the Bragg period for achieving a 1310nm stopband wavelength is around 240nm. This period is short enough to act as a sub-wavelength corrugation resulting in a homogenized effective material with respect to wavelengths around 1950 nm ($\lambda/n_{eff} \approx 870$ nm>>240nm=λ_{B-}) [19-22]. However, the large period grating needed for achieving a stopband around λ_{B+}=1950nm is simultaneously around 425 nm and can obviously give rise to diffractive effects [23] for short wavelengths around 1310nm. Fig. 3 shows the classical diffraction process diagram and the diffractive condition that can be expressed by equation (2):

$$K_{m,z} = K_{out,z} + qK_{\Lambda}, \qquad (q = 0, \pm 1, \pm 2, ...) \tag{2}$$

where K_m is the light waveguide mode wavevector, $K_{m,z}$ is the projection component of K_m in the z direction along propagation; K_{out} is the wavevector of the outgoing light from the waveguide into the cladding, $K_{out,z}$ is its projection component in z direction; K_Λ is the grating vector and q is the diffraction order. These related parameters can be expressed as follows:

$$\begin{cases} K_{m,z} = K_m = \dfrac{2\pi}{\lambda} n_{eff} \\ K_{out,z} = K_{out} \sin\theta = \dfrac{2\pi}{\lambda} n_c \sin\theta \\ K_\Lambda = \dfrac{2\pi}{\Lambda} \end{cases} \tag{3}$$

where n_c is the index of cladding and θ is the diffraction angle. Then, a further relationship can be derived from equation (2) and (3) to (4):

$$\Lambda \cdot (n_c \sin\theta - n_{eff}) = q\lambda \tag{4}$$

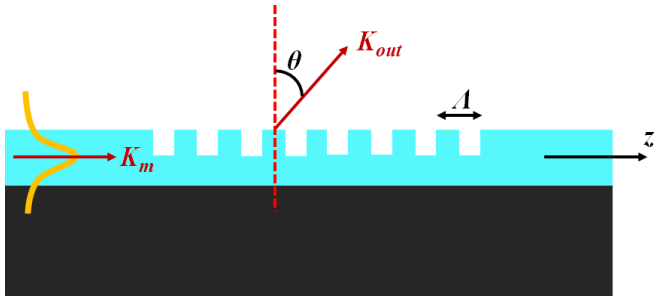

Fig. 3 Diagram for diffraction process.

In the typical studied example case made of an air cladded rib SOI waveguide, $\Lambda \approx 425$nm can be adopted for the outer Bragg grating period for 1950nm, which leads to the conclusion that -1st order diffraction effect can in principle happen at 1310nm wavelength with a diffraction angle $\theta \approx$ -16.25°. Obviously, this diffraction-based leakage channel can severely limit the target application of the realization of a low-loss dual wavelength rejection filter. It is thus necessary to circumvent this possible drawback.

In fact, it turns out that it is sufficient to move the outer gratings far enough away from the waveguide axis to effectively limit this penalty. This simple approach leads to inner and outer gratings of quite distinct coupling strengths due to the imposed distance of the outer gratings. This discrepancy can then be compensated for by an asymmetrical realization of the internal gratings, which deterministically reduces its coupling strength, and ultimately equalizes the properties of the two gratings and thus equalizes their bandwidths.

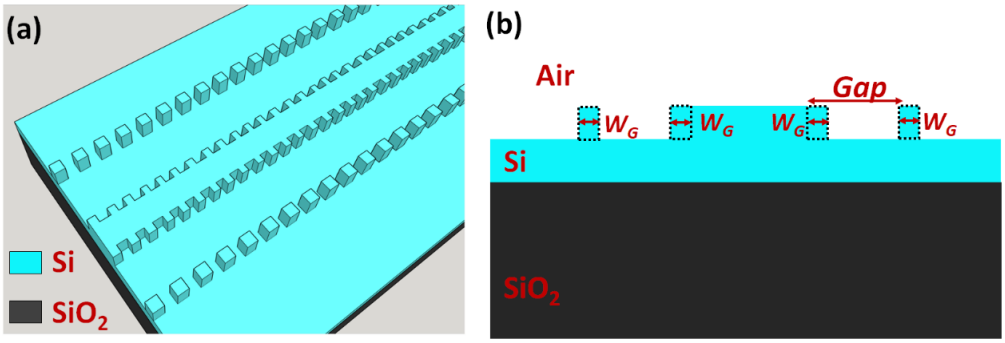

Fig. 4 (a) 3D schematic (b) 2D cross-section view of the rib waveguide with two sets gratings.

The practical implementation of this approach is illustrated in Fig. 4. With the SOI substrate parameters fixed, the main lines of the design are controlled by two parameters only, the lateral dimension of any corrugation (W_G) and the lateral distance from the rib to the outer gratings (*Gap*). The grating corrugation width is set as W_G = 50nm, thus remaining acceptable with respect to the fabrication process . Then the mode profiles at both target wavelengths are calculated as well as their corresponding effective mode areas through equation (5):

$$A_{eff} = \frac{(\int |E(x,y)|^2 dxdy)^2}{\int |E(x,y)|^4 dxdy} \tag{5}$$

where *E(x,y)* is the electrical field intensity and *x*, *y* are the dimensions along the waveguide cross-section. As expected, strongly different effective areas can be observed at λ_{B-} = 1310nm (0.1554 μm^2) and λ_{B+}=1950 nm (0.3614 μm^2) consistently with the mode profiles visible in Figs. 5 (a) and (b). The *Gap* parameter was investigated to figure out the spacing required to optically isolate the second gratings. It can be seen in Fig. 5 (c) that the effective index of the short-wavelength mode stabilizes beyond a gap of 400 nm. This is clearly the signature that the influence of the external corrugation on the short wavelength propagative mode then vanishes, thus favoring a reduction of the diffractive propagation loss level. An evaluation of this result is given hereafter in support of FDTD simulation.

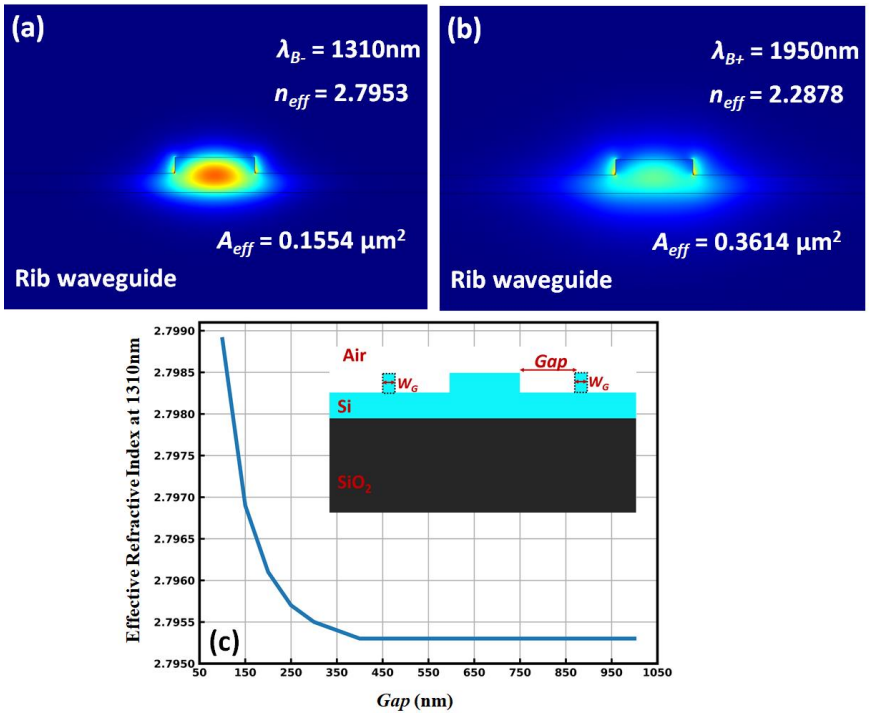

Fig. 5 (a) Mode profile at λ_{B-} = 1310nm. (b) Mode profile at λ_{B+}=1950nm.
(c) Relationship between effective refractive index at 1310nm and different *Gap* values.

To further realize dual identical narrowband Bragg filtering, the other key issue is to match the grating coupling coefficients of the two gratings. As well known, the bandwidth of a Bragg reflector can be derived from equation (6) [24]:

$$\Delta\lambda = \frac{\lambda_B}{\pi n_g}\sqrt{\kappa^2 + \left(\frac{\pi}{L}\right)} \tag{6}$$

where $\Delta\lambda$ is the bandwidth between the first nulls among the reflection spectrum, n_g is the group index of the waveguide modes, κ is the coupling coefficient provided by the grating structure, and L represents the total grating length. From equation (6), one can see that both the coupling coefficient and the Bragg reflector total length determine the Bragg bandwidth.

We estimated the coupling coefficients at λ_{B-} and λ_{B+} based on the proposed rib waveguide including two sets of gratings for *Gap* = 400nm of each a 50% filling factor. With all the determined parameters, the coupling coefficients could be estimated and derived through coupled mode theory (CMT) [25-27]. $\boldsymbol{\kappa_{B-}} = 6.73\times10^4\ m^{-1}$ and $\boldsymbol{\kappa_{B+}} = 1.13\times10^3\ m^{-1}$ were obtained, respectively. These different values are not surprising, as the two gratings are indeed positioned at very different distances from the center of the waveguide, but this situation does not allow, except for additional adjustment, an equalization of the bandwidths provided by each of the two gratings.

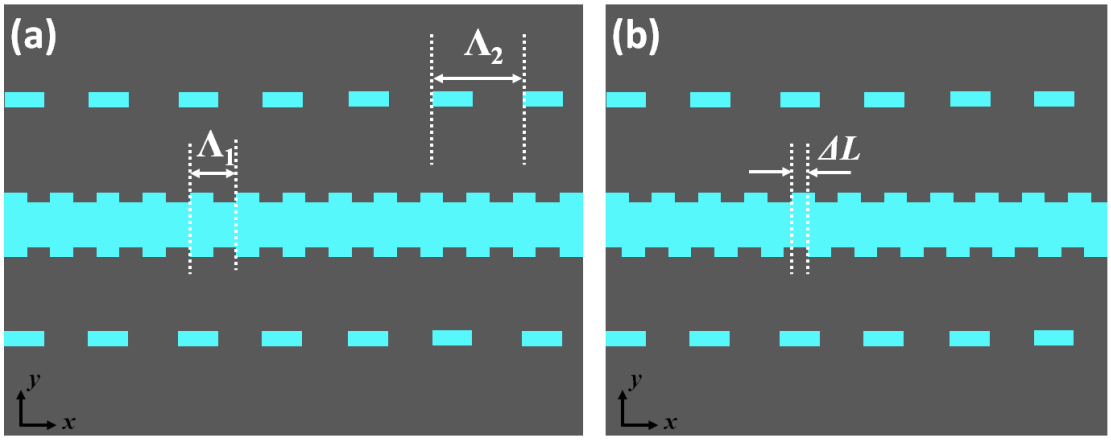

Fig. 6 Top view grating schematic (a) without misalignment; (b) with misalignment for inner grating.

To balance the two coupling coefficients, a misalignment between the left and right sides of the inner grating was further introduced [16,28] (see Figs. 6 (a) and (b)). The 500 nm wide SOI rib waveguide being single-mode at both wavelengths including ~1310nm, this asymmetry does not create mode conversion between guided modes. In case a ΔL misalignment is introduced between the two waveguide corrugated sidewalls, the grating coupling coefficient can be rewritten as follows:

$$\kappa = \left| \frac{\kappa_0}{2} + \frac{\kappa_0}{2}\exp(i \cdot 2\pi\Delta L / \Lambda) \right| = \kappa_0 \cos\left(\frac{\pi\Delta L}{\Lambda}\right) \tag{7}$$

where $\boldsymbol{\kappa_0}$ is the coupling coefficient for a normal grating structure (i.e. without misalignment), Λ the grating period, and $2\pi\Delta L/\Lambda$ is the phase offset between the two misaligned grating sidewall profiles. Accordingly, the inner grating coupling strength can be minimized to match the one of the outer grating. This approach is further developed in section 3 following.

3. Simulation results and discussion

To study and verify the proposed design strategy, device simulations based on 2.5D-FDTD [29] were implemented on ~1.3mm long structures. 2.5-FDTD was applied due to the very heavy cost of full 3D electromagnetic simulation of Bragg mirrors of several hundreds of µm lengths. It is based on collapsing the 3D geometry into a 2D set of effective indices calculated by relying on a variational approach that can be solved with 2D FDTD [30]. The main hypothesis of this approach is that there is a weak coupling between different supported vertical slab modes. The method allowed us to study the different Bragg mirrors with sufficient accuracy to validate their principles of operation and to compare the initial designs.

For clarity, all the related simulation parameters are listed in Table 1. Meanwhile, the grating offset value of the inner grating is noted as follows:

$$Offset = \frac{2\Delta L}{\Lambda_1} \cdot 90^{\circ} \tag{8}$$

Table 1

Parameters
Rib width: W_{rib} = 500nm
Rib height: H_{rib} = 100nm
Both gratings' single pillar width: W_g = 50nm
Inner grating's period: Λ_1 = 230nm
Single inner grating's length: $L_{g1} = 0.5 \cdot \Lambda_1$ = 115nm
Outer grating's period: Λ_2 = 426nm
Single outer grating's length: $L_{g2} = 0.5 \cdot \Lambda_2$ = 213nm
Number of inner grating periods: N_1 = 5556
Number of outer grating periods: N_2 = 3000
Dual wavelengths Bragg filter's total length: L = 1278μm

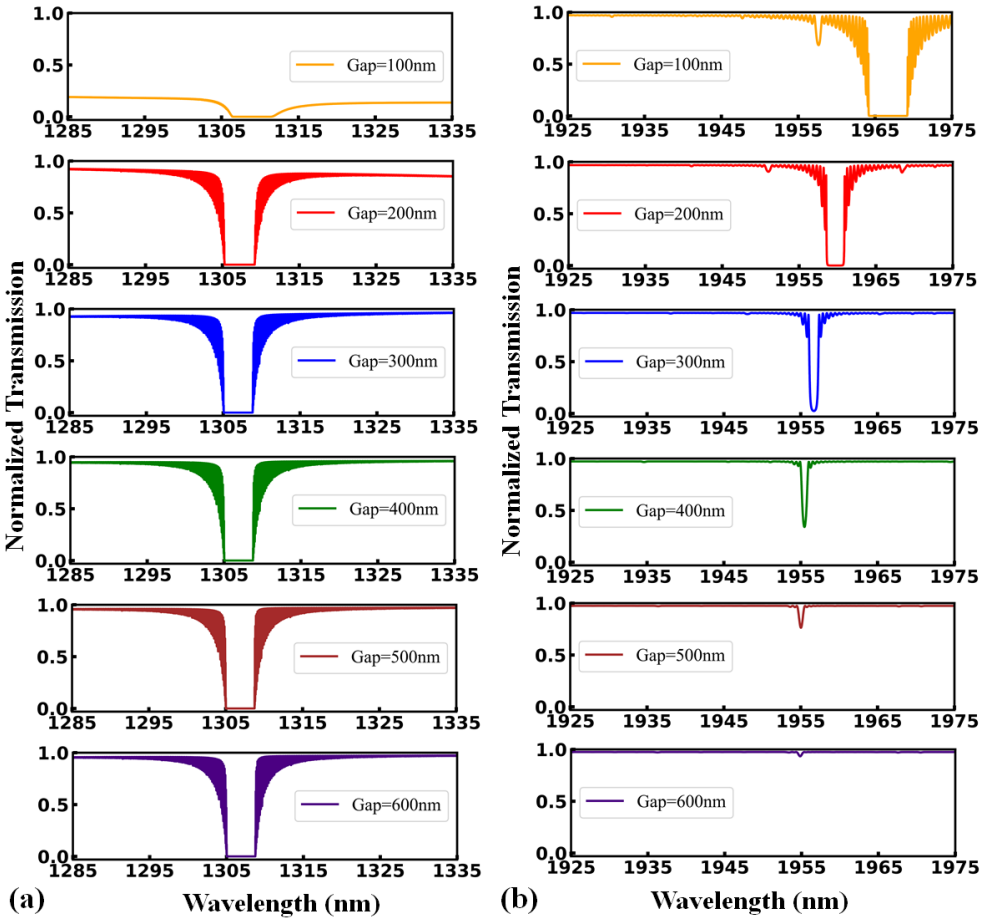

Fig. 7 2.5 FDTD-simulation results without offset on the inner grating while *Gap* varies from 100nm to 600nm with a 100nm step. (a) Normalized transmission near 1310nm wavelength; (b) Normalized transmission near 1950nm wavelength.

In a first step, no offset was introduced while the inter-grating distance value (*Gap*) was scanned from 100nm to 600nm. A series of transmission spectra were then acquired through 2.5D-FDTD simulation covering the 1200nm-2000nm range. The related results are plotted in Fig. 7(a) and Fig. 7(b) around 1310nm and 1950nm wavelengths, respectively. No attempt to apodize the spectral response of the studied filters [31] to minimize spectral sidelobes was tried as it was not the main purpose of the proposed study. From Fig. 7(a), it is observed that when *Gap* = 100nm, huge diffraction loss occurs around 1310nm, responsible for a low transmission level down to ~15%, while losses are effectively blocked by moving away from the outer gratings as early as *Gap* = 300nm. On the other hand, in Fig. 7(b),

the stopband around 1950nm becomes narrower and narrower with increasing *Gap* values, thereby progressively hiding the presence of a transmission dip around 1950nm wavelength. In view of previous achievements, the same fabrication constraints apply to these Bragg mirrors in terms of possible fabrication errors (under or over etching, stitching errors) [32]. Careful realization using DUV, or E-beam lithography and proper etching is necessary for their realization without affecting the principle of their implementation. As visible, the mirror reflectivity values at the Bragg wavelength do not reach 100% in several of the studied geometries. Previous works showed that narrow bandwidth Bragg filters with large reflectivity need long light pathways (e.g. [23] and equation (6)). To solutions could thus apply to improve the Bragg filter reflectivity levels: either increase the coupling strength of both gratings and match them in a second step while maintaining a constant grating overall length or, indeed, increase the Bragg filter lengths following previously proposed approaches to deepen the optical integration density [5].

In a second step, *Gap* was thus set to 400nm while the inner grating offset was scanned from 0° to 90°. As visible in Fig. 8, the stopband near 1310nm then becomes narrower and narrower with increasing offset values, thus bringing a confirmation of a grating asymmetry. Meanwhile, we verified that in all conditions the stop band near 1950nm keeps constant whatever the inner grating offset value is. Based on the acquired data, 3dB bandwidth values of all configurations were gathered (shown in Fig. 9(a)). As visible and understandable, the 3dB bandwidth of the short wavelength stopband decreases with the inner grating offset increase while the second stopband near 1950nm keeps a constant 3dB bandwidth. As observable in Fig. 9(b), which is a zoom-in view from the green dot line window of Fig. 9(a), an inner grating offset value around 84° was identified to provide two stopbands near 1310nm and 1950nm with equivalent 3dB bandwidth (~0.47nm).

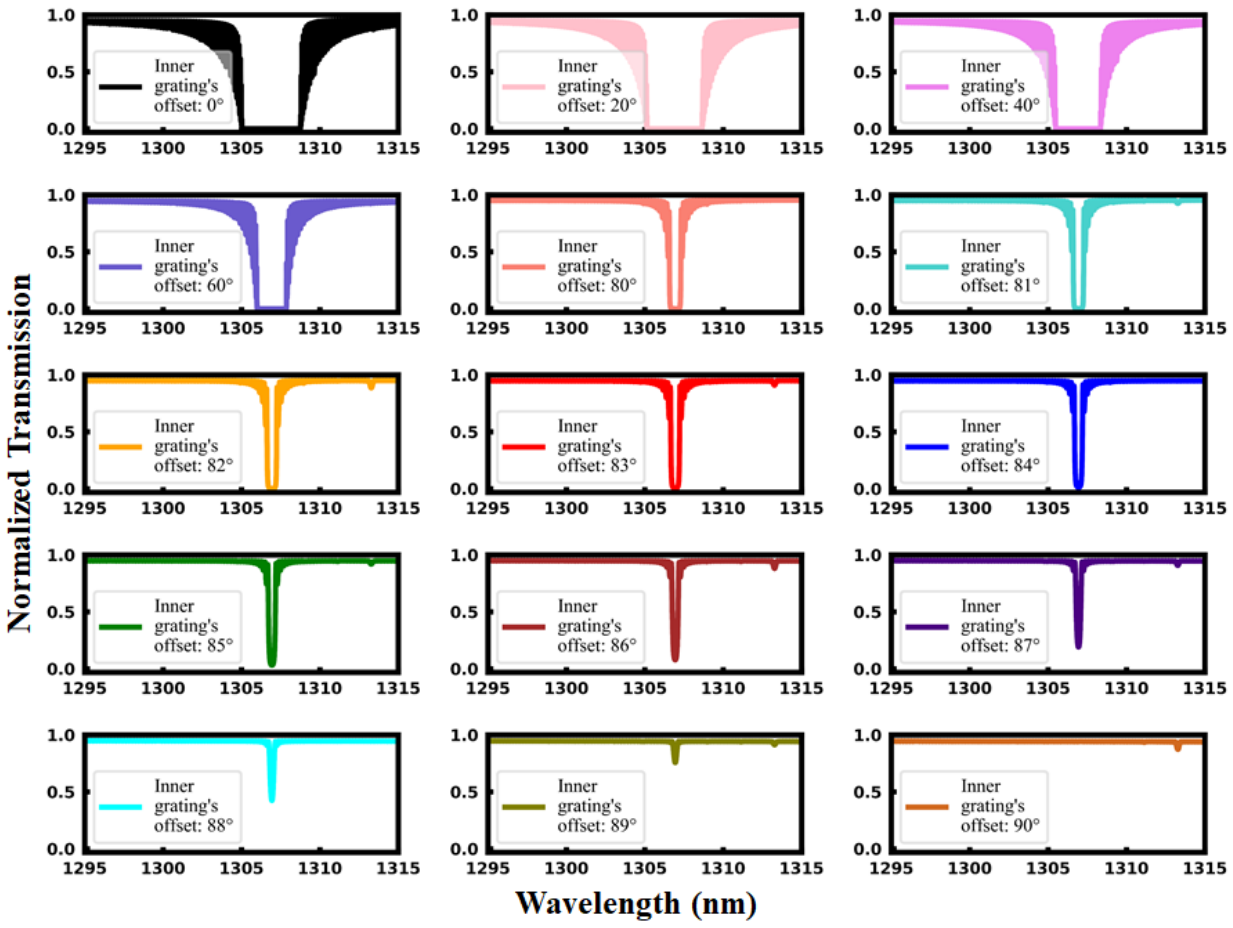

Fig. 8 2.5-FDTD simulation results with *Gap* = 400nm while the offset value varies from 0° to 90°: normalized transmission near 1310nm.

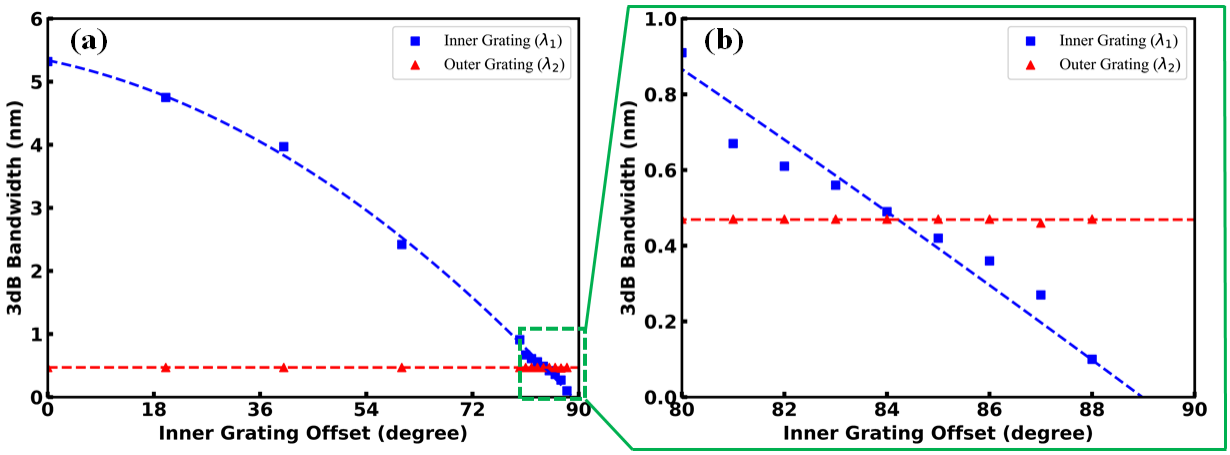

Fig.9 3dB bandwidth analysis derived from simulation results: (a) whole offset value window; (b) window near the cross-point between those two 3dB bandwidth stopbands

4. Conclusion

To conclude, a design strategy to successfully simultaneously realize a dual identical narrowband Bragg reflection filter at two widely separated wavelengths (~1310nm and ~1950nm in the investigated example study case) only requiring a single-etching fabrication process is proposed. A rib waveguide containing two sets of Bragg gratings was designed: the inner grating is close to the rib and owns a smaller period, thus providing a Bragg mirror effect for short wavelengths (~1310nm) while operating as a sub-wavelength effective index medium for longer wavelengths (~1950nm). The outer grating is located enough far away from the rib to avoid diffracting effects from the short wavelength compressed mode while providing a second Bragg stopband at and around ~1950nm. Diffraction effects being efficiently circumvented through a spatial lateral shift of the outer grating, the two sets Bragg gratings operate nearly independently. Additionally, a misalignment was introduced on the inner grating to balance the coupling strength coefficients between these two Bragg reflectors. Based on the determined parameters, simulation were carried to verify the feasibility of our proposed design and evaluate the needed offset value for the inner grating. As desired, the followed approach provided two narrow stopbands near 1310nm and 1950nm with identical 3dB bandwidth (~0.47nm). The proposed design strategy based on the silicon photonics platform relies on a single-etching fabrication process and presents potential applications in all situations where equal-bandwidth filtering is needed in on-chip communications and sensing.

Declaration of competing interest: The authors declare that they have no known competing financial interests or personal relationships that could have appeared to influence the work reported in this paper.

Acknowledgments: We thank the OpticAll ANR French national project as well as the CSC for supporting this work.

Reference

1. M. Pollnau, and J. D. B. Bradley, “Optically pumped rare-earth-doped Al2O3 distributed-feedback lasers on silicon [Invited],” Opt. Express **26**(18), 24164 (2018).
2. K. Bedard, A. D. Simard, B. Filion, Y. Painchaud, L. A. Rusch, and S. LaRochelle, “Dual phase-shift Bragg grating silicon photonic modulator operating up to 60 Gb/s,” Opt. Express, vol. 24, pp. 2413-2419, 2016.
3. O. Jafari, W. Shi, S. Larochelle, “Mach-Zehnder Silicon Photonic Modulator Assisted by Phase-Shifted Bragg Gratings,” IEEE Photon. Technol. Lett., 32(8) (2020) 445–448.
4. D. Oser, F. Mazeas, X. Le Roux, D. Pérez‐Galacho, O. Alibart, S. Tanzilli, L. Labonté, D. Marris‐Morini, L. Vivien, É. Cassan and C. Alonso‐Ramos, “Coherency-broken Bragg filters: overcoming on-chip rejection limitations,” Laser Photonics Rev. 13(8), 1800226 (2019).

5. S. Zamek, D. Tan, M. Khajavikhan, M. Ayache, M. Nezhad, and Y. Fainman, "Compact chip-scale filter based on curved waveguide Bragg gratings," Opt. Lett. 35, 3477-3479 (2010).
6. W. Zhang and J. Yao, "A fully reconfigurable waveguide Bragg grating for programmable photonic signal processing," Nature Comm., vol. 9, pp. 1396, 2018.
7. S. Khan and S. Fathpour, "Demonstration of complementary apodized cascaded grating waveguides for tunable optical delay lines," Opt. Lett., vol. 38, pp. 3914-3917, 2013.
8. H. Sun, Y. Wang and L. R. Chen, "Integrated Discretely Tunable Optical Delay Line Based on Step-Chirped Subwavelength Grating Waveguide Bragg Gratings," in Journal of Lightwave Technology, vol. 38, no. 19, pp. 5551-5560, 1 Oct.1, 2020.
9. P. Prabhathan, V. M. Murukeshan, Zhang Jing, and Pamidighantam V. Ramana, "Compact SOI nanowire refractive index sensor using phase shifted Bragg grating," Opt. Express 17, 15330-15341, 2009.
10. X. Wang, J. Flueckiger, S. Schmidt, S. Grist, S. T. Fard, J. Kirk, M. Doerfler, K. C. Cheung, D. M. Ratner, and L. Chrostowski, "A silicon photonic biosensor using phase-shifted Bragg gratings in slot waveguide," J. Biophotonics, vol. 6, no. 10, pp. 821-828, 2013.
11. J. Wang, and L. R. Chen, "Low crosstalk Bragg grating/Mach-Zehnder interferometer optical add-drop multiplexer in silicon photonics," Opt. Express, vol. 18, pp. 26450-26459, 2015.
12. Rui Cheng, Nicolas A. F. Jaeger, and Lukas Chrostowski, "Fully tailorable integrated-optic resonators based on chirped waveguide Moiré gratings," Optica 7, 647-657, 2020.
13. X. Wang, W. Shi, R. Vafaei, N. A. F. Jaeger, and L. Chrostowski, "Uniform and sampled Bragg gratings in SOI strip waveguides with sidewall corrugations," IEEE Phot. Tech. Lett., vol. 23, no. 5, pp. 290-292, 2011.
14. D. T. H. Tan, K. Ikeda, and Y. Fainman, "Cladding-modulated Bragg gratings in silicon waveguides," Opt. Lett. 34(9), 1357-1359, 2009.
15. Y.-J. Hung, K.-H. Lin, C.-J. Wu, C.-Y. Wang, and Y.-J. Chen, "Narrowband reflection from weakly coupled cladding-modulated Bragg gratings," IEEE J. Sel. Top. Quan. Electr., vol. 22, pp. 4402507, 2016.
16. T.-H. Yen, and Y.-J. Hung, "Narrowband dual-wavelength silicon waveguide Bragg reflectors," IEEE J. Lightw. Technol. 37(20), 5326-5332, 2019.
17. A. Napoli, N. Costa, J. K. Fischer, J. Pedro, S. Abrate, N. Calabretta, W. Forysiak, E. Pincemin, J. P. F. Gimenez, C. Matrakidis, G. Roelkens, and V. Curri, "Towards multiband optical systems," in Advanced Photonics 2018 (BGPP, IPR, NP, NOMA, Sensors, Networks, SPPCom, SOF), OSA Technical Digest (online) (Optical Society of America, 2018), paper NeTu3E.1.
18. W. H. Bragg and W. L. Bragg, The reflection of X-rays by crystals, Proc. R. Soc. Lond. A. 88 (605) (1913) 428-438.
19. Z. Tu, J. Zhang, C. Alonso-Ramos, X. L. Roux, L. Vivien, and E. Cssan, "Doubly Resonant Distributed Feedback Cavity with Controllable Wide Wavelength Separation," Opt. Commun. Vol. 494, 127064, 2021.
20. P. J. Bock, et al., "Subwavelength grating periodic structures in silicon-on-insulator: a new type of microphotonic waveguide," Opt. Express 18 (19) (2010) 20251-20262.
21. Robert Halir, et al., "Waveguide sub-wavelength structures: a review of principles and applications", Laser Photonics Rev. 9 (1) (2015) 25-49.
22. Z. Tu, D. Gao, M. Zhang, and D. Zhang, "High-sensitivity complex refractive index sensing based on Fano resonance in the subwavelength grating waveguide micro-ring resonator," Opt. Express 25 (17) (2017) 20911-20922.
23. D. Taillaert, W. Bogaerts, P. Bienstman, T. F. Krauss, P. Van Daele, I. Moerman, S. Verstuyft, K. De Mesel, and R. Baets, "An out-of-plane grating coupler for efficient butt-coupling between compact planar waveguides and single-mode fibers," IEEE J. Quantum Electron. 38(7), 949–955 (2002).
24. D. C. Flanders, H. Kogelnik, R. V. Schmidt, and C. V. Shank, "Grating filters for thin‐film optical waveguides," Appl. Phys. Lett. 24, 194 (1974).
25. T. E. Murphy, Design, Fabrication and Measurement of Integrated Bragg Grating Optical Filters, Ph.D. dissertation, Cambridge, MA, USA, 2001.
26. X. Wang, Silicon photonic waveguide Bragg gratings, Ph.D. dissertation, Univ. of British Columbia, Vancouver, Canada, 2013.
27. Z. Tu, J. Zhang, J. Rönn, C. Alonso-Ramos, X. Leroux, L. Vivien, Z. Sun, E. Cassan, "Potential for sub-mm long erbium-doped composite silicon waveguide DFB lasers," Sci. Rep. 10 (2020) 10878.
28. Xu Wang, Yun Wang, Jonas Flueckiger, Richard Bojko, Amy Liu, Adam Reid, James Pond, Nicolas A. F. Jaeger, and Lukas Chrostowski, "Precise control of the coupling coefficient through destructive interference in silicon waveguide Bragg gratings," Opt. Lett. 39(19), 5519-5522, 2014.
29. https://www.lumerical.com.
30. Manfred Hammer and Olena V. Ivanova, "Effective index approximation of photonic crystal slabs: a 2-to-1-D assessment", Optical and Quantum Electronics 41 (4), 267-283,2009)
31. J. T. Hastings, M. H. Lim, J. G. Goodberlet, and H. I. Smith, "Optical waveguides with apodized sidewall gratings via spatial-phase-locked electron-beam lithography," J. Vac. Sci. Technol. B (20), 2753–2757, 2002.
32. G Coppola, A Irace, A Cutolo, M Iodice,), "Effect of fabrication errors in channel waveguide Bragg gratings," Appl Opt. 20;38(9), 1752-8, 1999.